

submitted to *The Astrophysical Journal*

Direct Extragalactic Distance Determination Using X-Ray Scattering

B.T. Draine and Nicholas A. Bond

Princeton University Observatory, Peyton Hall, Princeton, NJ 08544;
draine@astro.princeton.edu, nbond@astro.princeton.edu

ABSTRACT

We examine the feasibility of using dust-scattered X-rays for direct determination of distances to nearby galaxies with bright background AGNs, QSOs, or GRBs. We show how the *Chandra* X-Ray Observatory could be used to determine the distance to M31 to an unprecedented absolute accuracy of $\sim 1\%$.

Subject headings: scattering – X-rays: ISM – galaxies: individual (LMC, M31, M81) – X-rays: general

1. Introduction

Distance measurement is one of the fundamental problems of astronomy. The distances to extragalactic objects are generally based on a “ladder”: (1) Luminosities of nearby (typically low-luminosity) stars are calibrated using trigonometric parallax. (2) Luminosities of more luminous stars (e.g., Cepheids, or stars at the tip of the red giant branch) are then determined by observing such stars in apparent proximity to analogues of the trigonometrically-calibrated low luminosity stars. (3) Distances to nearby galaxies are then determined by photometry of what are believed to be analogues of the luminous stars. Errors are contributed by difficulties of photometric calibration, possible physical differences between the calibrated luminous stars and the extragalactic targets, possible blending, and errors in corrections for interstellar extinction. Bonanos et al. (2003) conclude that distances to galaxies in the Local Group are today known to no better than 10–15%.

Geometric methods do exist for direct determination of extragalactic distances. Detached eclipsing binaries (DEBs) can be used (Paczyński 1997), with distances to individual DEBs in the LMC and SMC claimed to be accurate to 4–14% (Guinan et al. 1998; Fitzpatrick et al. 2003; Harries et al. 2003). Bonanos et al. describe a project to determine the distance to M31 using DEBs. The “light echo” of fluorescent emission from the ring around SN 1987A has been used to estimate the distance to the LMC (Panagia et al. 1991; Gould & Uza 1998 and references therein). Sparks (1997) has discussed the use of polarization in using light echoes to determine distances, and Xu et al. (1995) discuss using light scattered by dust to study the 3 dimensional structure of the ISM in front of SN 1987a. VLBI observations of the orbital motions of H₂O masers in the galaxy NGC 4258 allow the distance to be determined to an accuracy of 4% (Herrnstein et al. 1999) if it

is assumed that the transverse motions of the maser spots coincide with the physical motion of the gas.

Using time-delayed X-rays scattered by dust grains to estimate astronomical distances was originally proposed by Trümper & Schönfelder (1973). Here we demonstrate the feasibility of determining extragalactic distances by repeated X-ray imaging of a time-varying AGN or QSO located behind a foreground galaxy. The distant point source will be surrounded by a time-varying X-ray halo. Measurement of the time-delay of the halo, as a function of halo angle, allows the distance to the foreground galaxy to be determined. Being based purely on geometry, the method is essentially free of systematic uncertainties. The question is whether the time delay can be accurately measured using a realistic observing program – this is the focus of the present study.

The method depends on the X-ray scattering properties of interstellar dust grains, summarized in §2. The geometry of X-ray scattering by a foreground galaxy is described in §3. In §4 we consider some practical limits to the use of X-ray scattering to determine extragalactic limits. The method depends on variability of the X-ray source; in §5 we review the X-ray variability of AGNs, in §6 their availability on the sky..

In §7 we present a general procedure for determining the distance to a galaxy from repeated images of a background AGN and a field around it.

In §8 we discuss an observational program using the *Chandra* X-Ray Observatory to determine the distance to M31 using X-rays from the BL Lac object 5C 3.76. We carry out simulations to demonstrate the method, including photon-counting statistics and a realistic background. The reader interested primarily in the efficacy of this method may wish to go directly to Figure 8 and Table 1. A 5 Ms observational campaign with *Chandra* could determine the distance to M31 with an absolute uncertainty of $\sim 4\%$, using only X-ray observations; a 10 Ms campaign can reduce the uncertainty to $< 1\%$. We discuss how ancillary observations of CO and H I can be used to further improve the accuracy of the method.

We consider using background AGNs to determine the distances to other galaxies in §9, but conclude that M31 is the most favorable opportunity. In §10 we assess the feasibility of using a background gamma-ray burst to determine extragalactic distances, but conclude that with present X-ray telescopes this method will likely be limited to the LMC and SMC. Use of X-ray telescopes other than *Chandra* is considered in §11. Our conclusions are summarized in §12.

2. X-Ray Scattering by Dust

Interstellar dust grains scatter X-rays through small angles, as was first pointed out by Overbeck (1965), Slysh (1969), and Hayakawa (1970). Because of this scattering, an image of an X-ray point source includes a “halo” of X-rays that have been scattered by dust grains along the line of sight. First observed by Catura (1983) using the *Einstein* observatory, scattered X-ray halos have

since been studied by a number of telescopes, including *Einstein* (Mauche & Gorenstein 1986), *ROSAT* (Predehl & Schmitt 1995) and *Chandra* (e.g., Smith, Edgar, & Shafer 2002).

The scattered photons have a greater path length from source to observer than the unscattered photons. Therefore, if the source is time-variable, there will be a time-varying halo which is delayed relative to the observed variations in the point source. Because, for a given halo angle, the time delay depends on the distance to the source, Trümper & Schönfelder (1973) proposed that observations of time-variable scattered halos could be used to determine distances to variable X-ray sources. This effect has been used to estimate the distance to Cyg X-3 (Predehl, Burwitz, Paerels, & Trümper 2000) and to Nova Cygni 1992 (Draine & Tan, in preparation). Very recently, Vaughan et al. (2004) used the X-ray halo around GRB 031203 – seen through dust with $A_V \approx 3$ mag – to study the dust distribution toward $\ell = 255$ deg, $b = -4.6$ deg.

There continue to be uncertainties about the composition, size, and geometry of interstellar dust grains, but observations of X-ray scattering by dust are in reasonable agreement with grain models that are approximately consistent with a broad range of observational constraints (Draine 2003a). For a model of interstellar dust consisting of a size distribution of carbonaceous grains and silicate grains, the differential scattering cross section per H nucleon at X-ray energies can be approximated by (Draine 2003b)

$$\left(\frac{d\sigma_{\text{sca}}}{d\Omega} \right)_{\theta_s} \approx \frac{\sigma_{\text{sca}}}{2\pi\theta_s} \frac{d}{d\theta_s} \left[\frac{(\theta_s/\theta_{s,50})^2}{1 + (\theta_s/\theta_{s,50})^2} \right] , \quad (1)$$

where σ_{sca} is the total scattering cross section per H nucleon, θ_s is the scattering angle, and

$$\theta_{s,50} \approx 360'' \left(\frac{\text{keV}}{E} \right) \quad (2)$$

is the median scattering angle for photons of energy E . For this model the dust has a total scattering cross section given by

$$\frac{\tau_{\text{sca}}}{A_V} \approx 0.15 \left(\frac{E}{\text{keV}} \right)^{-1.8} \quad \text{for } 0.8 \text{ keV} \lesssim E \lesssim 10 \text{ keV} . \quad (3)$$

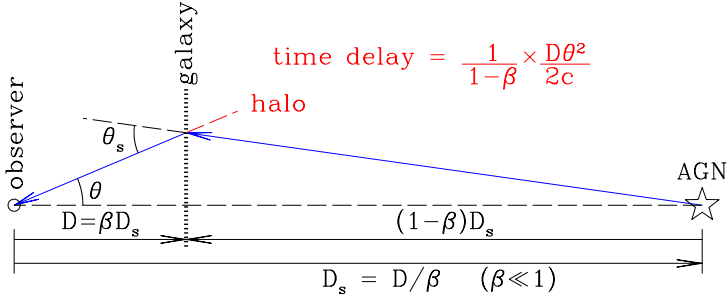
where A_V is the V band extinction, in magnitudes.

3. Scattering by Dust in a Foreground Galaxy

Suppose that we observe a point source with flux $F(t)$ located behind an intervening galaxy at distance D (see Fig. 1). Let the distance to the point source $D_s \gg D$. Then X-ray photons observed at “halo angle” θ have been scattered through an angle $\theta_s \approx \theta/(1 - \beta)$, where $\beta \equiv D/D_s \ll 1$.

Consider a region in the galaxy subtending solid angle $d\Omega$, at angular separation θ from the point source, with H column density N_{H} . The differential flux contributed by this region is

$$dH(t) = \left[\frac{F(t - \delta)}{(1 - \beta)^2} N_{\text{H}} \left(\frac{d\sigma_{\text{sca}}}{d\Omega_s} \right)_{\theta_s} + I_{\text{bg}} \right] d\Omega , \quad (4)$$



B. T. Draine 2004.07.14.2301

Fig. 1.— Geometry for single scattering of X-rays by dust in an intervening galaxy.

where δ is the increased light travel time for the scattered photons, and I_{bg} is background emission from unresolved sources and diffuse emission. For Euclidean space and $\theta \ll 1$, the time delay for the scattered photons is

$$\delta = \frac{1}{1-\beta} \frac{D\theta^2}{2c} = \frac{1.21 \times 10^7 \text{ s}}{1-\beta} \left(\frac{D}{\text{Mpc}} \right) \left(\frac{\theta}{100''} \right)^2 . \quad (5)$$

Now since $\theta_s = \theta/(1-\beta)$, we can write

$$\frac{d\sigma_{\text{sca}}}{d\Omega} = \frac{(1-\beta)^2 \sigma_{\text{sca}}}{2\pi\theta} \frac{d}{d\theta} \left[\frac{(\theta/\theta_{h,50})^2}{1 + (\theta/\theta_{h,50})^2} \right] , \quad \theta_{h,50} \equiv (1-\beta)\theta_{s,50} . \quad (6)$$

Thus

$$dH(t) = \left[\frac{F(t-\delta)N_{\text{H}}\sigma_{\text{sca}}}{2\pi\theta} \frac{d}{d\theta} \left[\frac{(\theta/\theta_{h,50})^2}{1 + (\theta/\theta_{h,50})^2} \right] + I_{\text{bg}} \right] d\Omega . \quad (7)$$

Consider annuli j , centered on the background point source, with inner radii subtending angles ψ_j , $j = 1, 2, \dots, J$. The flux from annulus j is

$$H_j(t) = F(t-\delta_j)m_j^0 + I_{\text{bg},j}\Omega_j , \quad (8)$$

where

$$m_j^0 \equiv \tau_{\text{sca},j} \left[\frac{(\psi_{j+1}/\theta_{h,50})^2}{1 + (\psi_{j+1}/\theta_{h,50})^2} - \frac{(\psi_j/\theta_{h,50})^2}{1 + (\psi_j/\theta_{h,50})^2} \right] \quad (9)$$

is the “magnification” of annulus j ,

$$\tau_{\text{sca},j} = N_{\text{H},j}\sigma_{\text{sca}} \quad (10)$$

is the X-ray scattering optical depth averaged over annulus j ,

$$\theta_j \equiv \left(\frac{\psi_j^2 + \psi_{j+1}^2}{2} \right)^{1/2} \quad (11)$$

is the r.m.s. value of θ for the annulus,

$$\Omega_j = \pi(\psi_{j+1}^2 - \psi_j^2) \quad (12)$$

is the solid angle of the annulus, and $I_{\text{bg},j}$ is the background averaged over the annulus. The average time delay for annulus j is

$$\delta_j = \frac{1}{1-\beta} \frac{D}{2c} \theta_j^2 \quad . \quad (13)$$

Note that portions of individual annuli can be “masked” – for example, if there are bright foreground point sources present in the image, or if a portion of the annulus falls beyond the detector boundary. In such cases, the discussion below is unaffected provided only that the scattering optical depth $\tau_{\text{sca},j}$ and the background $I_{\text{bg},j}$ averaged over the annulus includes zero for the unusable “masked” regions of the annulus. It is straightforward to continue to allow the background to vary from one annulus to another, but henceforth we will assume the background I_{bg} to be independent of j .

In the absence of other information, it is reasonable to assume the dust to resemble Milky Way dust (Draine 2003b), with scattering optical depth

$$\tau_{\text{sca},j} \approx A_{V,j} \times \left(\frac{\tau_{\text{sca}}}{A_V} \right) \quad , \quad (14)$$

Here $A_{V,j}$ is the visual extinction averaged over annulus j , and τ_{sca}/A_V is given in eq. (3).

4. Observability

Let T_{obs} be the time between the first and last observation. The largest useful halo angle is

$$\Theta_{\text{max}} = \left(\frac{2cT_{\text{obs}}}{D} \right)^{1/2} = 91'' \left(\frac{T_{\text{obs}}}{10^7 \text{ s}} \right)^{1/2} \left(\frac{\text{Mpc}}{D} \right)^{1/2} \quad ; \quad (15)$$

for halo angles $\theta > \Theta_{\text{max}}$ the time delay exceeds T_{obs} . The radius R of the dusty region of the galaxy defines a second characteristic angle

$$\theta_R \equiv \frac{R}{D} = 1030'' \left(\frac{R}{5 \text{ kpc}} \right) \left(\frac{\text{Mpc}}{D} \right) \quad . \quad (16)$$

Let $\Delta\theta$ be the angular resolution of the X-ray imager. Suppose that we wish to be able to determine the distance D to within a fractional error ϵ , given a sufficient number of counts. There are 3 different constraints which determine the maximum distance D for which this technique for distance determination is feasible.

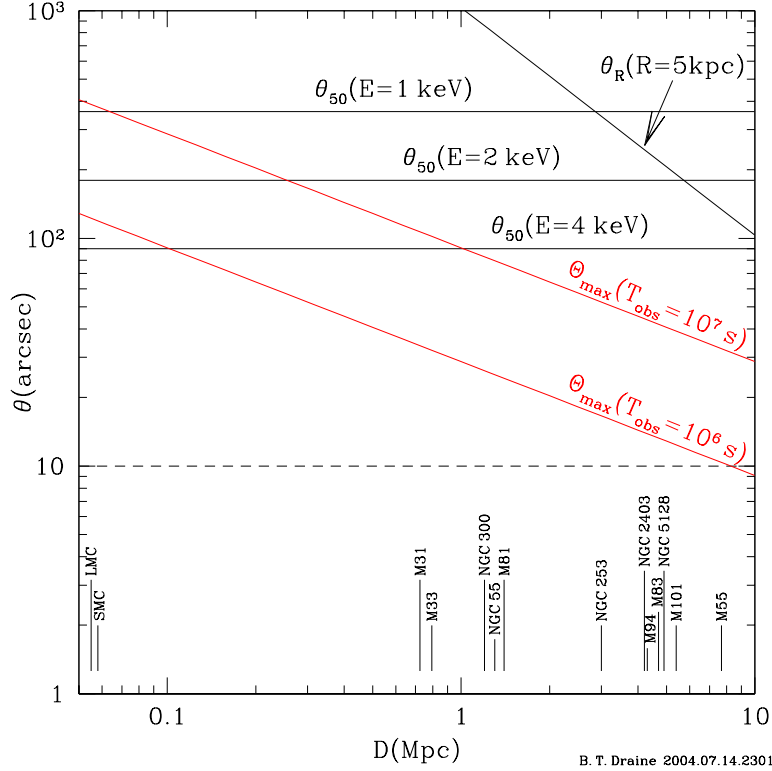


Fig. 2.— Characteristic angles as a function of distance D : θ_R is the angle subtended by 5 kpc. $\Theta_{\max}(T_{\text{obs}})$ is the angle corresponding to a time delay T_{obs} . $\theta_{50}(E)$ is the median scattering angle for photon energy E .

1. Even if the time delay δ_j were measured precisely for some annulus j , accurate determination of the distance $D = 2c\delta_j/\theta_j^2$ requires measurement of the halo angle θ_j to fractional accuracy $\epsilon/2$. Because the distribution of dust in the galaxy will be irregular, we cannot assume the dust to be uniformly distributed within an annulus. Thus determination of the scattering angle to a fractional accuracy $\epsilon/2$ requires an annulus width $\psi_{j+1} - \psi_j < \epsilon\theta_j$. The annulus width is at least equal to $\Delta\theta$; thus $\Delta\theta < \epsilon\Theta_{\max}$, or

$$D < \frac{2\epsilon^2 c T_{\text{obs}}}{(\Delta\theta)^2} = 0.827 \text{ Mpc} \left(\frac{\epsilon}{0.01} \right)^2 \left(\frac{T_{\text{obs}}}{10^7 \text{ s}} \right) \left(\frac{1''}{\Delta\theta} \right)^2 . \quad (17)$$

2. The maximum halo angle is limited by the angular extent of the dusty portion of the galaxy. Measurement of halo angles to accuracy ϵ would require $\Delta\theta < \epsilon\theta_R$, or

$$D < \frac{\epsilon R}{\Delta\theta} = 10 \text{ Mpc} \left(\frac{\epsilon}{0.01} \right) \left(\frac{R}{5 \text{ kpc}} \right) \left(\frac{1''}{\Delta\theta} \right) . \quad (18)$$

3. Suppose τ_{sca} is uniform for $r < R$. The count rate of scattered photons then varies as

$$H_{\text{sca}}(t) = \sum_{j=1}^J H_j(t) \approx \left[\frac{[\min(\Theta_{\max}, \theta_R)/\theta_{h,50}]^2}{1 + [\min(\Theta_{\max}, \theta_R)/\theta_{h,50}]^2} \right] F \tau_{\text{sca}} . \quad (19)$$

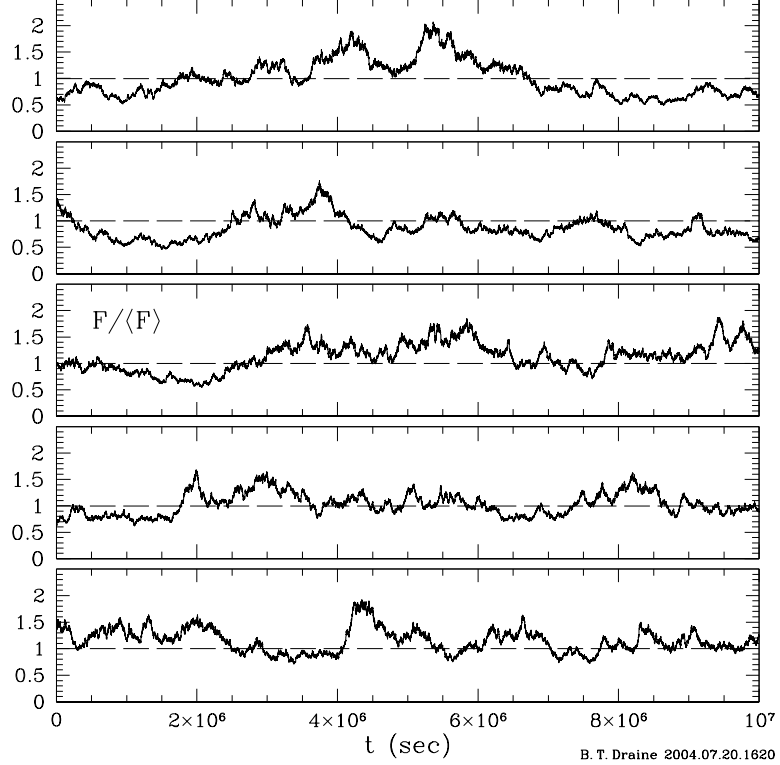


Fig. 3.— Flux F relative to long-term average flux $\langle F \rangle$ for 5 independent realizations of light curves with variability amplitude $A = 0.3$ and correlation time $\tau = 10^6$ s, generated as described in Appendix A.

From Figure 2 we see that for $1 \text{ Mpc} \lesssim D \lesssim 50 \text{ Mpc}$ and $T_{\text{obs}} < 10^7$ s, $\Theta_{\text{max}} < \theta_R \ll \theta_{h,50}$, so that the halo count rate $H_{\text{sca}} \propto F\tau_{\text{sca}}/D$, showing that the method is increasingly challenging as the distance D is increased.

5. X-Ray Variability of AGNs

We simulate the X-ray light curve of an AGN with the simple stochastic model described in Appendix A. The model light curve is controlled by three parameters: the average count rate $\langle F \rangle$, a characteristic correlation time τ , and a variability amplitude parameter A . To choose realistic values of these parameters, we consider the X-ray lightcurves obtained for AGNs using EXOSAT (Lawrence & Papadakis 1993) and RXTE (Markowitz et al. 2003) and for QSOs using ROSAT (Ezoe et al. 2002). Based on these studies, we adopt a correlation time $\tau \approx 10^6$ s as representative (see Appendix A).

The amplitude of variation can be characterized by F_{var} , the square root of the variance normalized to the mean flux. Six Seyfert 1 galaxies observed by Markowitz et al. had values of F_{var} ranging from 0.22 to 0.39, corresponding to the parameter A ranging from 0.22 to 0.38. We take

$A = 0.3$ as typical for AGNs. Five independent examples of synthetic light curves are shown in Figure 3.

6. Density of Background AGNs

The ROSAT North Ecliptic Pole Survey (Gioia et al. 2003), covering an 80.7 deg^2 area, detected 54 AGNs with $0.5\text{-}2\text{keV}$ flux (corrected for absorption) greater than $2.5 \times 10^{-13} \text{ erg cm}^{-2} \text{ s}^{-1}$. The catalog is approximately consistent with

$$\left(\frac{dN(E S_E > S)}{d\Omega} \right)_{E=1\text{keV}} \approx 1.6 \left(\frac{S}{10^{-13} \text{ erg cm}^{-2} \text{ s}^{-1}} \right)^{-3/2} \text{ deg}^{-2} , \quad (20)$$

where S_E is the energy flux per unit photon energy E . Expressed in terms of count rate \dot{N} for the back-illuminated CCDs of the *Chandra* Advanced CCD Imaging Spectrometer (ACIS-S BI) detector, we estimate¹

$$\frac{dN(\dot{N} > \dot{N}_{\min})}{d\Omega} \approx 1.6 \left(\frac{\dot{N}_{\min}}{.04 \text{ cnt s}^{-1}} \right)^{-3/2} \text{ deg}^{-2} . \quad (21)$$

If we have a foreground galaxy of area $\Delta\Omega$, then we have a 50% probability of having at least one background source with a *Chandra* count rate exceeding

$$\dot{N}_{\min} = .04 \text{ cnt s}^{-1} \left(\frac{1.6 \text{ deg}^{-2} \Delta\Omega}{\ln 2} \right)^{2/3} = .07 \text{ cnt s}^{-1} \left(\frac{\Delta\Omega}{\text{deg}^2} \right)^{2/3} . \quad (22)$$

7. Distance Determination

Here we describe a simple method for estimating the distance from the observed X-ray images. Suppose that we have K images; image k covers “time bin” k extending from $t_{1,k}$ to $t_{2,k}$, with $\Delta t_k \equiv t_{2,k} - t_{1,k}$. The images are time-ordered, with $t_{2,k} \leq t_{1,k+1}$. Each image is divided into circular annuli $j = 1, \dots, J$ centered on the background source, with the innermost annulus exterior to the p.s.f.

We now shift from discussion of fluxes to counts. Let N_k be the number of counts from the point source in time bin k . We assume that for each annulus j , the photon arrival times t_{arr} are known; if not actually known, a random number generator is used to assign arrival times t_{arr} for each detected photon within each integration interval.

¹To estimate the *Chandra* ACIS-S BI count rates, we note that the OGLE source J005719.84-722533.5 with $\langle E S_E \rangle_{1\text{keV}} = 1.13 \times 10^{-13} \text{ erg cm}^{-2} \text{ s}^{-1}$, seen through $N_{\text{H}} = 1.5 \times 10^{22} \text{ cm}^{-2}$ has a count rate $\langle \dot{N} \rangle \sim 0.041 \text{ s}^{-1}$ (Dobrzycki et al. 2003).

The time delay for annulus j is $\delta_j = \alpha\theta_j^2$, with α an unknown parameter to be determined. There will be “background” counts due to noise in the detector, cosmic ray events, and unresolved celestial sources. Let $I_{\text{bg}}A_{\text{eff}}\Omega_j$ be the background count rate in the telescope in annulus j . We will suppose that this background I_{bg} (taken here to be uniform over the region of interest) is not known a priori, but needs to be estimated from the observations.

For a trial value of the time delay parameter α , let the “exposure fraction” $f_{jk}(\alpha)$ be the fraction of the time interval $[t_{1,k} + \alpha\theta_j^2, t_{2,k} + \alpha\theta_j^2]$ during which the target was observed. Obviously $f_{jk} < 1$ for $t_{2,k} + \alpha\theta_j^2 > t_{2,K}$, and $f_{jk} = 0$ for $t_{1,k} + \alpha\theta_j^2 \geq t_{2,K}$; $f_{jk} < 1$ can also result from gaps in the observing campaign.

Let $H_{jk}(\alpha)$ be the actual number of counts in annulus j during time interval $[t_{1,k} + \alpha\theta_j^2, t_{2,k} + \alpha\theta_j^2]$ (obviously, $H_{jk} = 0$ when $f_{jk} = 0$). From the H_{jk} , we construct the total (halo + background) counts in time bin k ,

$$G_k(\alpha) = \sum_{j=1}^J H_{jk}(\alpha) \quad . \quad (23)$$

For a trial value of the background I_{bg} , we use the observations to estimate the “magnification” of each annulus,

$$m_j(\alpha, I_{\text{bg}}) = w_j(\alpha) \sum_{k=1}^K [H_{jk}(\alpha) - b_{jk}(\alpha, I_{\text{bg}})] \quad , \quad (24)$$

$$b_{jk}(\alpha, I_{\text{bg}}) \equiv I_{\text{bg}}A_{\text{eff}}\Omega_j f_{jk}(\alpha) \Delta t_k \quad , \quad (25)$$

$$w_j(\alpha) \equiv \left[\sum_{k=1}^K f_{jk}(\alpha) N_k \right]^{-1} \quad . \quad (26)$$

For each trial (α, I_{bg}) we calculate

$$\chi^2(\alpha, I_{\text{bg}}) \equiv \sum_{k=1}^K W_k(\alpha) \frac{[G_k(\alpha) - M_k(\alpha, I_{\text{bg}})N_k - B_k(\alpha, I_{\text{bg}})]^2}{\sigma_k^2(\alpha, I_{\text{bg}})} \quad , \quad (27)$$

where

$$B_k(\alpha, I_{\text{bg}}) \equiv \sum_{j=1}^J b_{jk} \quad , \quad (28)$$

$$M_k(\alpha, I_{\text{bg}}) \equiv \sum_{j=1}^J m_j(\alpha, I_{\text{bg}}) f_{jk}(\alpha) \quad , \quad (29)$$

$$W_k(\alpha) \equiv \frac{G_k(\alpha)}{\sum_{\ell=1}^K G_{\ell}(\alpha)} \quad . \quad (30)$$

The effective halo magnifications $M_k(\alpha, I_{\text{bg}})$ depend on k because at early times the outer annuli are not usable (i.e., have $f_{jk} = 0$) since the scattered light coming from them corresponds to the

unobserved point source light curve at $t < t_{1,1}$. The normalized weights W_k , with $\sum W_k = 1$, are included to place greater weight on time bins where more counts have been observed.

The denominator σ_k^2 in eq. (27) is calculated assuming photon counting statistics (see Appendix D):

$$\sigma_k^2(\alpha, I_{\text{bg}}) = G_k(\alpha) + N_k M_k^2 - 2(N_k^2 + N_k^2 M_k + N_k M_k) S_k + (4N_k^2 + N_k) S_k^2 + (N_k^2 + N_k)(T_k + U_k) - 2N_k V_k , \quad (31)$$

where the estimated halo magnification $M_k(\alpha, I_{\text{bg}})$ is given by eq. (29), the weighting factors $w_j(\alpha)$ are given by eq. (26), and

$$S_k(\alpha, I_{\text{bg}}) \equiv \sum_{j=1}^J m_j w_j f_{jk}^2 , \quad (32)$$

$$T_k(\alpha, I_{\text{bg}}) \equiv \sum_{j=1}^J (w_j f_{jk})^2 \sum_{\ell=1}^K (m_j f_{j\ell} N_\ell + b_{j\ell}) , \quad (33)$$

$$U_k(\alpha, I_{\text{bg}}) \equiv \sum_{\ell=1}^K N_\ell \left(\sum_{j=1}^J m_j w_j f_{jk} f_{j\ell} \right)^2 , \quad (34)$$

$$V_k(\alpha, I_{\text{bg}}) \equiv \sum_{j=1}^J w_j f_{jk} b_{jk} . \quad (35)$$

We require that $\sum_k f_{jk} N_k \gg 1$ so that the statistical analysis of Appendix D be valid.

There are $K \gg 1$ halo epochs. We expect the function $\chi^2(\alpha, I_{\text{bg}})$ to have a minimum; let this be at $(\alpha_*, I_{\text{bg}*})$. If the parameters α and I_{bg} are set to their true values, then $\langle \chi^2 \rangle = 1$ (see Appendix D). We adjust α and I_{bg} to minimize χ^2 , but have a large number of annuli and epochs; we expect $\chi^2(\alpha_*, I_{\text{bg}*}) \approx 1$ if the only errors are due to Poisson statistics. Our best estimate for the distance is

$$D_* = 2(1 - \beta)c\alpha_* . \quad (36)$$

While we do not claim the above methodology to be the optimal distance estimator – there may be alternative approaches that are less sensitive to Poisson noise – we demonstrate below by direct simulation that the method is capable of determining the distance for realistic data sets.

8. Determination of the Distance to M31: Simulations

8.1. Dusty Disk

The dusty portion of the disk of M31 subtends a solid angle $\sim 0.8 \text{ deg}^2$ (Xu & Helou 1996; Schmidtobreick et al. 2000), corresponding to a projected area $= 1.10 \times 10^{45} \text{ cm}^2$ for an assumed

distance $D \approx 770$ kpc (Freedman & Madore 1990; van den Bergh 2000). The total dust and gas mass have been estimated to be $(2.4 \pm 0.7) \times 10^7 M_{\odot}$ and $M_{\text{H}} \approx 2.5 \times 10^9 M_{\odot}$ within this disk (Xu & Helou 1996, corrected to $D = 770$ kpc). Thus $N_{\text{H}} = 1.95 \times 10^{21} \text{ cm}^{-2}$. Using $N_{\text{H}}/A_V = 1.87 \times 10^{21} \text{ cm}^{-2}$, we estimate $A_V \approx 1.0$ averaged over the 0.8 deg^2 region.

The disk thickness of ~ 200 pc is negligible compared to the distance D , so we can treat the disk as a scattering sheet. From eq. (5) we see that a time delay of 10^7 s corresponds to an angle $\theta \approx 100''$, so opposite sides of the scattering region will differ in distance to us by $\Delta D \approx 2D\theta \sin i \approx 0.001D \sin i$, where i is the inclination. Inclination effects are therefore negligible, and the scattering region can be idealized as a thin sheet in the plane of the sky.

8.2. 5C 3.76

For $\Omega = 0.8 \text{ deg}^2$, eq. (21) would predict a 50% probability of at least one background source with *Chandra* count rate $> 0.06 \text{ cnt s}^{-1}$. Nature has provided at least 1 background AGN above this value:² 5C 3.76 [= WSTB 37W051 = RX J0040.2+4050; RA 00h40m13.7s, DEC 40d50m05s (J2000)] – a compact nonthermal radio source about $40'$ (~ 9 kpc projected distance) from the center of M31. It was detected as an X-ray source by Einstein and *ROSAT*, and is classified as a BL Lac object (Perlman et al. 1996; Laurent-Muehleisen et al. 1999; Nilsson et al. 2003), of unknown redshift. 5C 3.76 is located behind $N(\text{H I}) = 1.34 \times 10^{21} \text{ cm}^{-2}$ of atomic H (Dickey & Brinks 1993). If we assume that $\sim 75\%$ of the gas is atomic, with the balance either ionized or molecular, and assume that the dust is similar to Milky Way dust (with $N_{\text{H}}/A_V \approx 1.87 \times 10^{21} \text{ cm}^{-2}$), then we estimate $A_V \approx 1.0$ mag for this region of M31.

Supper et al. (2001) reported a *ROSAT* PSPC 0.5-2 keV count rate of 0.124 cnt s^{-1} , corresponding to $ES_E(1 \text{ keV}) \approx 3 \times 10^{-12} \text{ erg cm}^{-2} \text{ s}^{-1}$. 5C 3.76 was observed at 16 different epochs by the *Chandra* HRC, with a mean count rate³ 0.122 cnt s^{-1} (Williams et al. 2004). With 5C 3.76 located behind $N(\text{HI}) \approx 1.34 \times 10^{21} \text{ cm}^{-2}$, the X-ray spectrum is presumably strongly absorbed below 0.45 keV. If the flux were in 1.5 keV photons, for which the ACIS-S camera has $A_{\text{eff}} \approx 600 \text{ cm}^2$ (vs. $\sim 200 \text{ cm}^2$ for the HRC) the ACIS-S on-axis count rate would be $\sim 0.4 \text{ cnt s}^{-1}$; we adopt this as the estimated count rate.

BL Lac-type objects are generally variable. The X-ray flux from 5C 3.76 was in fact observed to be variable by Williams et al.; the flux dropped by a factor ~ 1.7 between 2000-09-11 and 2000-10-12. Given its X-ray brightness, variability, and location, 5C 3.76 is an attractive background

²Somewhat outside the dusty disk, the background AGN Mrk 957 has a ROSAT count rate of 0.076 cnts^{-1} – about 60% of 5C 3.76 – and is known to show X-ray variability (Supper et al. 2001). Located just inside the D_{25} countour of M31 (~ 20 kpc from the center), the dust extinction will be substantially lower than for 5C 3.76, making Mrk 957 less attractive than 5C 3.76 as a background source for determination of the distance to M31.

³5C 3.76 = object s1-75 was located 9.9 arcmin off-axis in the HRC observations.

source to use to determine the distance to M31. The variability spectrum of 5C 3.76 is not well-determined; we provisionally approximate it by our stochastic model with $\tau = 10^6$ s and $A = 0.3$ (see Figure 3).

Because the redshift of 5C 3.76 is not known, we do not know the value of $\beta \equiv D/D_s$. However, it is probably safe to provisionally assume a redshift $z > 0.03$, in which case $D_s > 125$ Mpc, $\beta \lesssim 0.006$, and we can assume the factor $(1 - \beta) \approx 1$ in eq. (36). Therefore even if the redshift is not known, the resulting uncertainty in the distance determination will be less than 0.6% provided $z > 0.03$. A program to determine the distance to M31 using X-rays from 5C 3.76 should, however, include optical spectroscopy of 5C 3.76 to attempt to determine its redshift.

8.3. Diffuse Background

Diffuse emission in M31 was measured by *ROSAT* (West et al. 1997). At $\sim 40'$ from the center (along the major axis), unresolved sources contribute a *ROSAT* 0.5-2.0 keV count rate $\sim 7 \times 10^{-8}$ cnt s $^{-1}$ arcsec $^{-2}$. Taking into account the greater effective area of the *Chandra* ACIS-S camera (600 cm 2 at 1.5 keV, vs ~ 150 cm 2 for *ROSAT* PSPC) we estimate a *Chandra* ACIS-S background count rate $\sim 2.8 \times 10^{-7}$ cnt s $^{-1}$ arcsec $^{-2}$.

XMM-Newton recently observed diffuse X-ray emission from a region $14' - 45'$ NE of the nucleus of M31, along the major axis (Trudolyubov et al. 2004), allowing an independent determination of the unresolved background. At $\sim 30'$ from the nucleus, the diffuse 0.2–1.5 keV XMM count rate is $\sim 9.2 \times 10^{-7}$ cnt s $^{-1}$ arcmin $^{-2}$ (the lowest contour shown by Trudolyubov et al); from the radial variation seen by West et al. we estimate the count rate at $40'$ to be lower by a factor ~ 0.75 . Taking into account the smaller effective area of *Chandra*⁴ we estimate that the diffuse emission will contribute a *Chandra* count rate $I_{\text{bg}}^0 A_{\text{eff}} \approx 3 \times 10^{-7}$ cnt s $^{-1}$ arcsec $^{-2}$, in excellent agreement with the background estimated from the *ROSAT* observations.

8.4. Simulations

With 5C 3.76 in mind, we simulate observations of a point source with mean 0.5 – 5 keV count rate $\langle \dot{N} \rangle = 0.4$ cnt s $^{-1}$, with a stochastic light curve generated following Appendix A with variability amplitude $A = 0.3$ and correlation time $\tau = 10^6$ s. We take the X-rays to have a characteristic energy $E = 1.5$ keV, and approximate the disk of M31 as a uniform scattering screen with a scattering optical depth $\tau_{\text{sca}} = 0.072$ for the X-ray photons (corresponding to $A_V = 1$ mag). The scattering phase function for the X-rays is assumed to be that estimated for Milky Way dust

⁴At 1.5 keV, *Chandra* ACIS-S and XMM have effective areas of ~ 600 and ~ 1300 cm 2 , respectively.

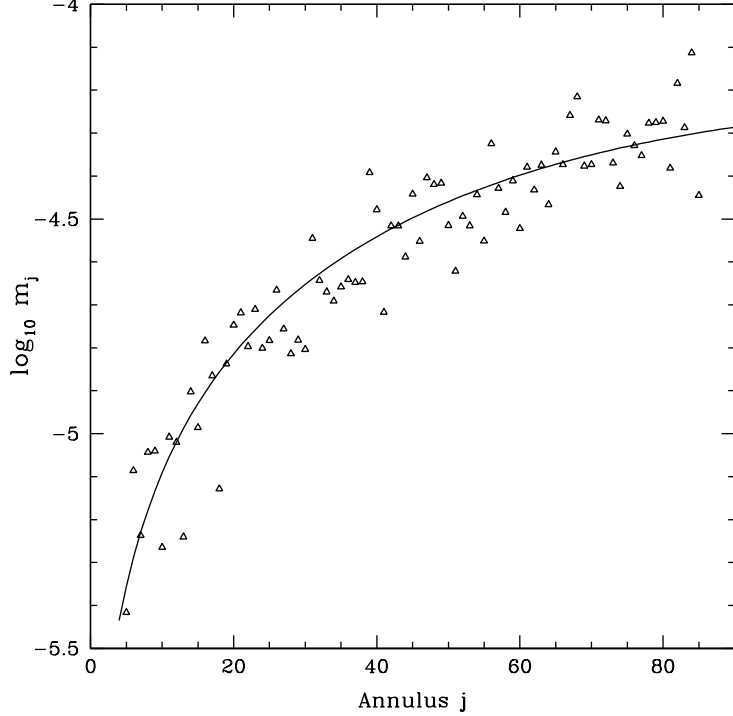


Fig. 4.— Symbols: estimated values of m_j vs. annulus number j for a randomly-selected simulation with $T_{\text{obs}} = 7 \times 10^6$ sec, for the best-fit distance D and background I_{bg} . Solid line: m_j^0 used in the simulation. m_j is largest for large j because the outer annuli (with $\Delta\theta = 1''$) have larger area.

at 1.5 keV (see eq. 1,2).⁵ The time delay parameter is set to $\alpha_0 = D_0/(2c)$, where $D_0 = 770$ kpc [and we take $\beta = 0$ in eq. (13)].

In addition to the scattered X-rays, we assume a uniform background with a count rate $I_{\text{bg}}^0 A_{\text{eff}} = 3 \times 10^{-7}$ cnt s⁻¹ arcsec⁻².

For simplicity, we simulate observing campaigns without gaps, with continuous exposures $T_{\text{obs}} = 3, 5, 7$, and 10 Ms. For each case we perform 10^3 independent simulations.

For the 10 Ms observing campaign, the maximum useful scattering angle [see eq. (15)] is $\Theta_{\text{max}} = 104''$. For 1.5 keV photons, the median scattering angle is $\theta_{50} = 240''$. The mean count rate for scattered photons within $100''$ of the point source will be $\sim 0.4 \cdot 0.072 \cdot (100/240)^2 / [1 + (100/240)^2] = 0.0043$ cnt s⁻¹, only $\sim 45\%$ of the background count rate within this region.

⁵While the total scattering cross section [eq. (3)] varies as $\sim E^{-1.8}$, the differential scattering cross section at $\theta < \theta_{s,50}$ [see eq. (2)] is nearly independent of E (see Fig. 8 of Draine 2003b). The observations considered here are at $\theta < \theta_{s,50}$, and thus our estimated count rates for scattered photons are insensitive to the assumed energy spectrum of the point source.

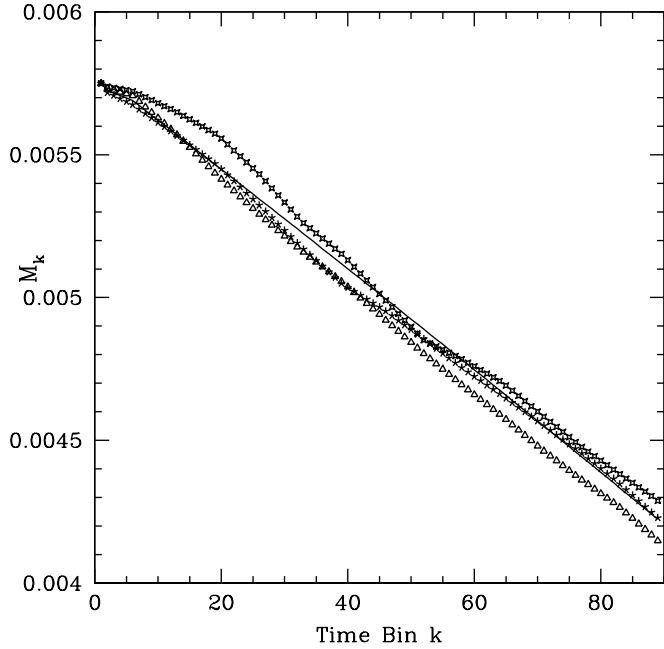


Fig. 5.— Effective total halo magnification M_k for time bin k . Solid line: M_k^0 for the simulations. Symbols: M_k for three randomly-selected simulations with $T_{\text{obs}} = 7 \times 10^6$ s.

We use uniform time bins of width $\Delta t = 5 \times 10^4$ s, so that the point-source counts per time bin $\langle N_k^0 \rangle \approx 2 \times 10^4$. The halo annuli are constructed as described in Appendix B, with minimum annular width of $\Delta\theta = 1''$, giving $J = 101$ annuli within $104''$.

For each simulated data set, we construct the delay-corrected halo light curve $G_k(\alpha)$ for a trial value of the time delay parameter α . For different trial values of I_{bg} , we calculate $\chi^2(\alpha, I_{\text{bg}})$ using eq. (27). We repeat the procedure for different trial values of α , and adopt the values $(\alpha_*, I_{\text{bg}*})$ for which χ^2 is minimized.

For small values of T_{obs} , the number of halo counts is small, Poisson fluctuations are very substantial, and α_* may be far from the “true” value α_0 . Because the amount of useful data decreases as the trial value of α (i.e., D) is increased, Poisson noise may result in a false minimum of χ^2 for large values of D . Because we have a-priori limits on the plausible range of distances to M31, we search for the minimum of χ^2 only over the range $[0.78D_0, 1.22D_0]$. In the event that this minimum occurs outside the range $[0.8D_0, 1.2D_0]$, we reject the distance determination altogether. Such rejections are, however, relatively rare, especially for the longer simulated campaigns. In a real observing campaign, the observations would be continued to accumulate data and eliminate such spurious results. For 5 Ms exposures, we had only 27 rejections in 1000 simulations; for the

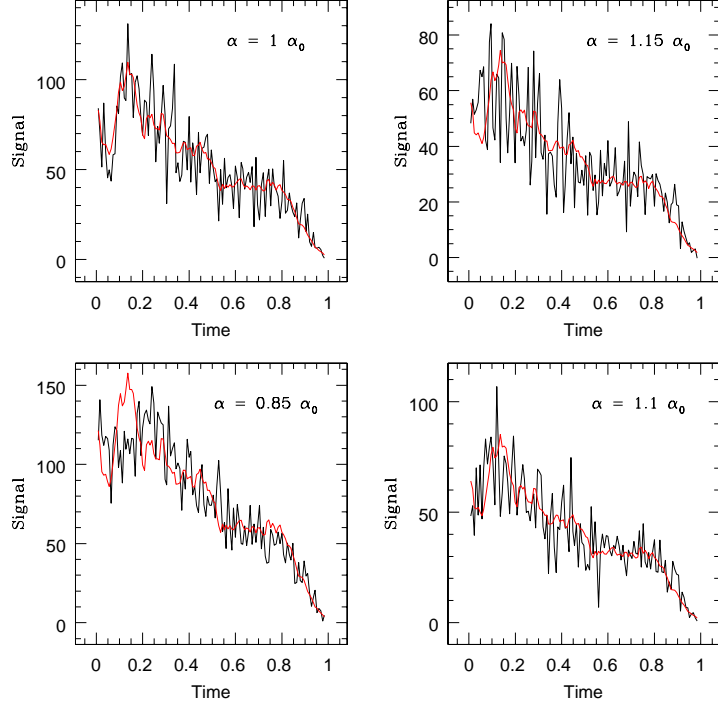


Fig. 6.— $(G_k - B_k)$ (black) and $N_k M_k$ (red) for four different trial values of α , for a simulation with $T_{\text{obs}} = 5\text{Ms}$. At late times $(G_k - B_k)$ and $N_k M_k$ go to zero because only the innermost annuli provide data. To the eye, $N_k M_k$ and $(G_k - B_k)$ appear to be more similar for the true delay $\alpha = \alpha_0$ than for the trial values $0.85\alpha_0$, $1.1\alpha_0$, or $1.15\alpha_0$, but the Poisson noise is large.

10 Ms campaign, we had 0 rejections in 1000 simulations.

The method involves estimation of the annular magnifications m_j from the observations. Figure 4 shows the m_j estimated from a 7 Ms simulation. Because of Poisson statistics, the m_j are quite noisy. However, the M_k (see eq. 29 and Figure 5) are much better behaved, as expected.

Our method seeks the time delay that minimizes the difference between $(G_k - B_k)$ and $N_k M_k$. Figure 6 shows these two functions of time for one $T_{\text{obs}} = 5\text{Ms}$ simulation, for four trial values of α . To the eye, $N_k M_k$ and $(G_k - B_k)$ do appear to be more similar for the true delay $\alpha = \alpha_0$ than for the trial values $0.85\alpha_0$, $1.1\alpha_0$, or $1.15\alpha_0$, but the Poisson noise is obviously large. Our χ^2 statistic is intended to quantify the difference between $(G_k - B_k)$ and $N_k M_k$, where $\langle \chi^2 \rangle = 1$ for the true time delay.

In Figure 7 we show χ^2 vs D/D_0 for different trial values of I_{bg} , for 4 independent simulations with $T_{\text{obs}} = 7 \times 10^6 \text{s}$. The value of I_{bg} giving the $\chi^2(\alpha)$ with the lowest minimum ranges from $0.87I_{\text{bg}}^0$ to $1.09I_{\text{bg}}^0$ – the background estimate is accurate to about 10%. It is also apparent that the location of the minimum is not highly sensitive to the estimate of I_{bg} . Most importantly, it is

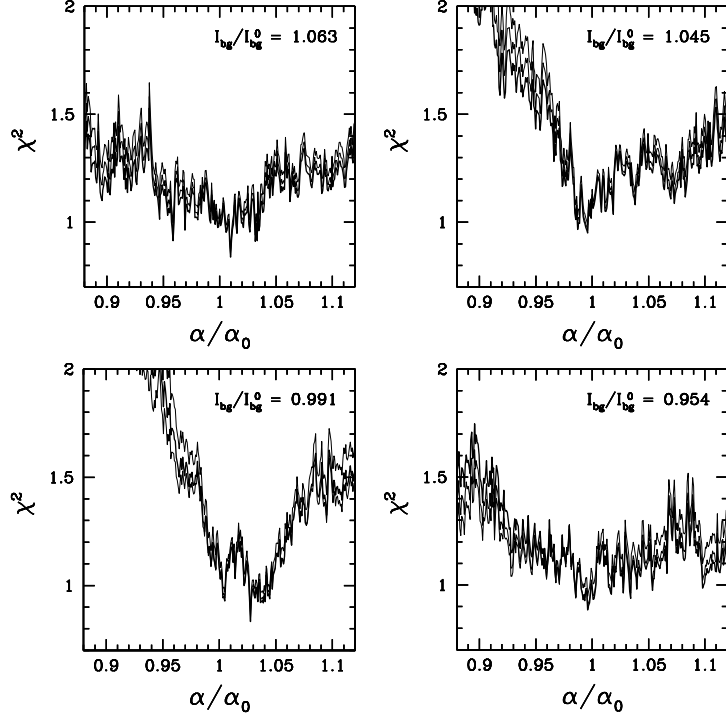


Fig. 7.— χ^2 vs D/D_0 for 4 randomly selected simulations with $T_{\text{obs}} = 7 \times 10^6$ s. In each case we show $\chi^2(\alpha)$ for 3 trial values of I_{bg} : $0.92I_{\text{bg}}^0$, $1.08I_{\text{bg}}^0$, and the background that leads to the lowest minimum of $\chi^2(\alpha)$. For each case we give the estimate $I_{\text{bg},*}$ as a fraction of I_{bg}^0 .

seen that the minimum α_* is very close to the true value α_0 – within $\sim 3\%$ – for each of these four simulations.

Histograms of D_*/D_0 are shown in Figure 8 for each of the 4 values of T_{obs} . Table 1 gives the median, 68% confidence interval, and rejection fraction, for 4 different values of T_{obs} . For the shortest observing campaign, $T_{\text{obs}} = 3$ Ms, the simulations result in a fairly broad distribution of derived distances D , with about 83 of the experiments resulting in “rejection”. For the 917 nonrejected cases, the median $D/D_0 = 1.026$, and the 68% confidence interval extends from about $0.967 < D/D_0 < 1.137$, i.e., “one σ ” uncertainties of $^{+11.1\%}_{-5.9\%}$.

As the observing time T_{obs} increases, the amount of useful data increases as $\sim T_{\text{obs}}^2$, because it is possible to use scattered halo photons at larger angular separations from the point source. As a result, the accuracy of the the distance determination improves rapidly. As seen from Figure 8 and Table 1, it appears to be possible to determine the absolute distance to M31 to within $\pm 1\%$ with a 10 Ms observing campaign with *Chandra*.

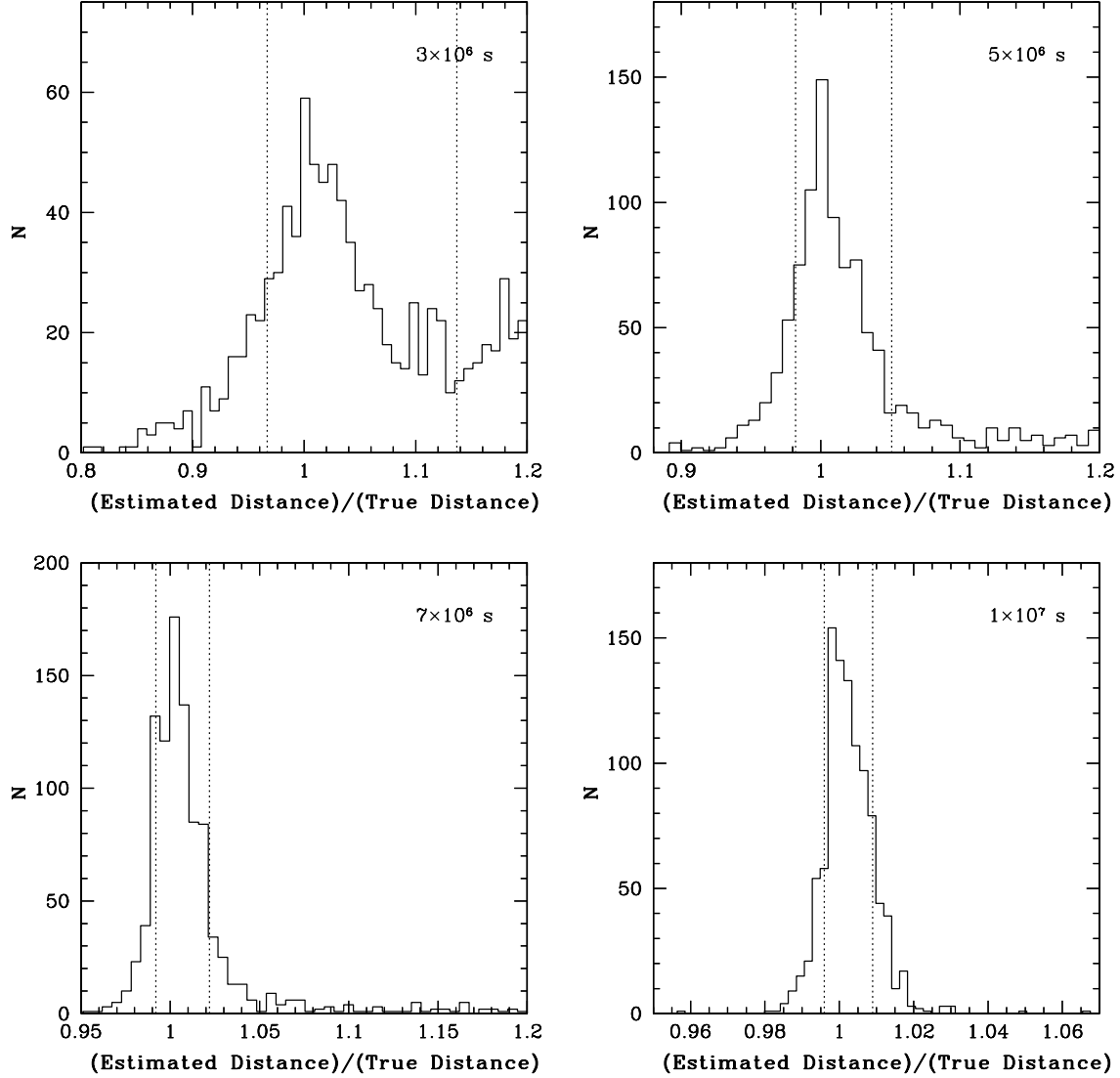


Fig. 8.— Histograms showing distribution of D_{est}/D_0 for M31, where D_{est} is the estimated distance, for simulations with $T_{\text{obs}} = 3, 5, 7$, and 10 Ms . In each case, we show results for 10^3 simulations. Distance estimates differing from the true distance by more than 20% are rejected (see text). Of the remaining distance estimates, 68% fall between the dotted lines, 16% above, and 16% below; the dotted lines can be loosely understood as $\pm 1\sigma$ uncertainties in the distance estimation.

8.5. Discontinuous Observing

Our discussion assumed, for simplicity, continuous observations of M31. Realistic orbital and scheduling considerations would require gaps in the observing. The methodology presented in §7 can be applied to observing campaigns that include gaps.

Table 1: Results for Simulated M31 Observing Campaigns

T_{obs}	D_{est}/D_0 ^a	rejects
3 Ms	$1.026^{+0.111}_{-0.059}$	8.3%
5 Ms	$1.007^{+0.044}_{-0.025}$	2.7%
7 Ms	$1.005^{+0.017}_{-0.013}$	2.1%
10 Ms	$1.002^{+0.007}_{-0.006}$	< 0.1%

^a68% confidence interval based on 10^3 independent simulations (see text), rejecting simulations where the distance estimate differs from the true distance by more than 20%.

The simplest approach would be to use only the time intervals for which the AGN was observed, and only the counts from annuli j with arrival times t_{arr} such that $t_{\text{arr}} - \alpha\theta_j^2$ was a time when the AGN was observed. This approach would, however, have the disadvantage of discarding halo counts for which $t_{\text{arr}} - \alpha\theta_j^2$ falls in a gap when the AGN was not observed.

A better approach, if individual gaps are not too long, would be to interpolate to estimate the AGN counts N_k for time intervals falling in the gaps in the observations. This can be accomplished using the procedure described by Press, Rybicki, & Hewitt (1992). Using these interpolated counts in the same way as the actual counts N_k , one could use the same procedure described above to minimize $\chi^2(\alpha, I_{\text{bg}})$ to find the distance D .

Provided the interruptions in observing are sufficiently brief ($\lesssim 1$ day) that the AGN lightcurve can be reliably interpolated, discontinuous observing should be almost as effective as continuous observations with the same total exposure time.

8.6. Using Multiwavelength Data

We have shown above that it is possible to determine the distance to M31 using *only* X-ray imaging. In particular, the X-ray data alone is used to estimate the “magnification” m_j of each annulus, which is proportional to the amount of interstellar dust present in the annulus.

Imaging at other wavelengths can also provide information on the distribution of interstellar dust. Note that the scattering zones j need not be complete annuli – the annuli can be subdivided in the event that the dust distribution is nonuniform. Indeed, if a portion of the annulus were known to be dust-free, this should be masked off, as it would contribute Poisson noise from the background but no signal. If the dust distribution over the annulus is appreciably nonuniform, it may be advantageous to subdivide the annulus into subannuli, with low and high dust densities. If

H I and CO observations are used to estimate the surface density of gas, the magnification

$$m_j = f(\theta) \left(\frac{\tau_{\text{sca}}}{N_{\text{H}}} \right) \Omega_j [X_{\text{H}} I_j(\text{H 21cm}) + 2X_{\text{CO}} I_j(\text{CO 2.6mm})] \quad (37)$$

where $f(\theta)$ is the angular distribution function for X-ray scattering⁶ at halo angle θ , Ω_j is the solid angle of (sub)annulus j , I_j (line) is the line intensity in a spectral line averaged over (sub)annulus j , X_{H} is the conversion factor from 21cm line intensity to H I column density, and X_{CO} is the conversion factor from CO line intensity to H₂ column density.

There are at least two different ways in which this information could be used:

1. If the angular resolution and signal/noise ratio of the 21cm and CO images is sufficient, and a good estimate for $f(\theta)$ is in hand, we could use eq.(37) [rather than eq. (24)] to estimate the m_j for the (sub)annuli, but with the scaling factor $\tau_{\text{sca}}/N_{\text{H}}$ to be determined. Now instead of trial values of α and I_{bg} , we would instead consider trial values of α and $\tau_{\text{sca}}/N_{\text{H}}$; for each $(\alpha, \tau_{\text{sca}}/N_{\text{H}})$ pair, the background I_{bg} is estimated from

$$I_{\text{bg}}(\alpha, \tau_{\text{sca}}/N_{\text{H}}) = \frac{\sum_{k=1}^K \left(G_k(\alpha) - N_k \sum_{j=1}^J m_j f_{jk} \right)}{A_{\text{eff}} \sum_{k=1}^K N_k \sum_{j=1}^J \Omega_j f_{jk}} \quad (38)$$

Using this value of I_{bg} , $\chi^2(\alpha, \tau_{\text{sca}}/N_{\text{H}})$ is then calculated for the trial values of α and $\tau_{\text{sca}}/N_{\text{H}}$. The best estimates of α and $\tau_{\text{sca}}/N_{\text{H}}$ are then found by minimizing $\chi^2(\alpha, \tau_{\text{sca}}/N_{\text{H}})$.

2. Alternately, the magnifications $m_j(\alpha, I_{\text{bg}})$ estimated from the X-ray data alone [eq. (24)] could be compared to the m_j estimated from eq. (37), by computing an error function

$$\chi_d^2 \equiv \sum_j \frac{[m_j(\text{eq.24}) - (\tau_{\text{sca}}/N_{\text{H}}) s_j]^2}{\sigma^2(m_j)} \quad (39)$$

$$s_j \equiv f(\theta) \Omega_j [X_{\text{H}} I_j(\text{H 21cm}) + 2X_{\text{CO}} I_j(\text{CO 2.6mm})] \quad (40)$$

$$\frac{\tau_{\text{sca}}}{N_{\text{H}}} = \frac{\sum_{j=1}^J m_j(\alpha, I_{\text{bg}}) s_j / \sigma^2(m_j)}{\sum_{j=1}^J s_j^2 / \sigma^2(m_j)} ; \quad (41)$$

$\sigma^2(m_j)$ is the variance in m_j due to Poisson statistics [see eq. (D23)]:

$$\sigma^2(m_j) \approx m_j (w_j)^2 \sum_k f_{jk} N_k + (w_j)^2 \sum_k b_{jk} + (m_j w_j)^2 \sum_k f_{jk}^2 N_k . \quad (42)$$

For the wrong estimate of the distance, the estimated magnifications m_j will be systematically in error. Thus $\chi_d^2(\alpha)$ should have a minimum at the true value of the time delay parameter α_0

⁶With normalization $\int f(\theta) 2\pi \sin \theta d\theta = (1 - \beta)^{-2} \approx 1$.

For method (1) to be useful, it is necessary to have imaging data at angular resolutions smaller than the larger of (a) the annular widths ($1''$), or (b) the angular scale over which the dust surface density varies. It would be useful to have 21cm and CO interferometric imaging of this $4' \times 4'$ region of M31. In principle, the dust could be observed directly using SCUBA on the JCMT (HPBW of $7.5''$ at $450\mu\text{m}$), or MIPS on the Spitzer Space Telescope ($\sim 30''$ at $160\mu\text{m}$), but the angular resolution of these instruments is probably insufficient to trace the dust variation from annulus to annulus.

The best use of multiwavelength data will depend on its angular resolution and signal/noise ratio. We do not undertake any such simulations here. However, it is clear that this additional information can only improve the distance determinations. If an observing campaign is undertaken with *Chandra*, use of multiwavelength data should be further investigated to make best use of the *Chandra* observing time.

9. Other Galaxies: LMC, SMC, and M81

With an H I mass $3.1 \pm 0.6 \times 10^8 M_\odot$ (Luks & Rohlfs 1992), the LMC has $\langle N_{\text{H}} \rangle = 1 \times 10^{21} \text{ cm}^{-2}$ over $\Omega = 40 \text{ deg}^2$. The dust/gas ratio in the LMC is $\sim 40\%$ of the Milky Way value, hence we estimate $\langle A_V \rangle \approx 0.21 \text{ mag}$, and $\tau_{\text{sca}} \approx 0.015(E/1.5 \text{ keV})^{-1.8}$. What is required is a bright background source. Dobrzański et al. (2003) report 5 new X-ray QSOs behind the SMC, the brightest of which has a *Chandra* count rate 0.041 cnt s^{-1} . Over the 40 deg^2 area of the LMC, eq. (22) leads us to expect the brightest background AGN to have $ES_E \approx 2 \times 10^{-12} \text{ erg cm}^{-2} \text{ s}^{-1}$, with a *Chandra* count rate $\dot{N} \approx 0.8 \text{ cnt s}^{-1}$. This is only twice the count rate for 5C 3.79, and τ_{sca} is likely to be a factor of two lower than for 5C 3.79, so the actual halo brightness for an AGN behind the LMC may not be higher than for 5C 3.79 behind M31. The reduced distance ($D = 66 \text{ kpc}$ for the LMC) allows observation of the time-delayed halo out to $\sim 112''(T_{\text{obs}}/10^6 \text{ sec})^2$, but an accurate distance determination would still require a substantial observing campaign, and ultimately would be limited by the uncertain three-dimensional geometry of the LMC. In many ways M31 is a more attractive candidate for X-ray distance determination using AGNs.

As discussed in §4, distance determination using X-ray halos can be applied to galaxies beyond M31, but with increasing difficulty. M81, at a distance $D = 1.4 \text{ Mpc}$, is perhaps the next most likely candidate. Immler & Wang (2001) present ROSAT observations of M81. Aside from the nucleus of M31, the brightest source in the field is source X9, located 12.2 arcmin E of the nucleus (5 kpc projected separation). Variable (with an amplitude exceeding a factor of 2.5; Immler & Wang 2001), with a ROSAT PSPC count rate of 0.20 cnt s^{-1} , and located in a region of M81 with $N(\text{H I}) \approx 3 \times 10^{21} \text{ cm}^{-2}$ (Immler & Wang 2001), X9 would be suitable for distance determination if it were a distant background source, but Wang (2002) argues that X9 is an intermediate-mass black hole associated with M81. At this time there are no known bright background sources that would allow X-ray distance determination to M81 with existing observational capabilities.

10. Using X-Rays from Gamma-Ray Bursts

Suppose a gamma-ray burst (GRB) occurs behind a nearby galaxy (e.g., LMC, SMC, or M31), with fluence F_0 in 1–2 keV X-rays. We approximate the GRB X-rays as a single short-duration pulse. The galaxy is approximated as a uniform thin screen with X-ray scattering optical depth τ_{sca} . The dust is assumed to have the scattering phase function of Milky Way dust for 1.5 keV X-rays [see eq. (1,2)].

The fluence in scattered X-rays is

$$dF_{\text{sca}} = F_0 \tau_{\text{sca}} \frac{1}{\sigma_{\text{sca}}} \frac{d\sigma_{\text{sca}}}{d\Omega} 2\pi\theta d\theta \quad (43)$$

$$\approx F_0 \tau_{\text{sca}} \frac{d(\theta/\theta_{h,50})^2}{[1 + (\theta/\theta_{h,50})^2]^2} / \quad (44)$$

Since the geometric time delay $t = \alpha\theta^2$, we find

$$dF_{\text{sca}} = F_0 \tau_{\text{sca}} \frac{dt/t_{h,50}}{[1 + t/t_{h,50}]^2} , \quad (45)$$

where

$$t_{h,50} = \alpha\theta_{h,50}^2 = 3.9 \times 10^6 \text{ s} \left(\frac{D}{56 \text{ kpc}} \right) . \quad (46)$$

We now suppose that we image over the interval $(t - \Delta t/2, t + \Delta t/2)$. The scattered photons will be observed as a ring with radius $\theta = (t/\alpha)^{1/2}$ and width $(\Delta\theta)_{\text{obs}} = \max[\Delta\theta, \Delta t/(2\alpha\theta)]$, where $\Delta\theta$ is the angular resolution of the X-ray imager. The number of scattered photons counted in the ring will be

$$N_r \approx F_0 \tau_{\text{sca}} A_{\text{eff}} \frac{\Delta t/t_{h,50}}{(1 + t/t_{h,50})^2} \quad (47)$$

$$\approx 23 \cdot \left(\frac{F_0}{10^2 \text{ cm}^{-2}} \right) \left(\frac{\tau_{\text{sca}}}{0.015} \right) \left(\frac{56 \text{ kpc}}{D} \right) \left(\frac{240''}{\theta_{h,50}} \right)^2 \left(\frac{A_{\text{eff}}}{600 \text{ cm}^2} \right) \frac{\Delta t/10^5 \text{ s}}{(1 + t/t_{h,50})^2} , \quad (48)$$

where A_{eff} is the effective area of the X-ray imager.

The ring will therefore be detected with a signal-to-noise ratio

$$S/N \approx \frac{N_r}{(N_r + N_{\text{bg}})^{1/2}} , \quad (49)$$

where the number of background counts in the ring is

$$N_{\text{bg}} = I_{\text{bg}} A_{\text{eff}} 2\pi\theta (\Delta\theta)_{\text{obs}} \Delta t . \quad (50)$$

As an example, consider a GRB with a 0.5 – 5 keV X-ray fluence $F_0 = 10^3 \text{ photon cm}^{-2}$, located behind a region of the LMC ($D = 56 \text{ kpc}$) with $A_V = 0.2$ ($\tau_{\text{sca}} \approx 0.015$). A $\Delta t = 2 \times 10^4 \text{ s}$

exposure with the *Chandra* ACIS ($A = 600 \text{ cm}^2$), taken at a time $t = 10^6 \text{ s}$ (when the ring radius is $\theta = 122''$) will have $\Delta\theta = 1.22''$, and will detect $N_r = 29$ counts due to the scattered halo. If $I_{\text{bg}} A_{\text{eff}} = 3 \times 10^{-7} \text{ cnt s}^{-1} \text{ arcsec}^{-2}$, there will be $N_{\text{bg}} \approx 6$ background counts in the annulus, and the ring will be detected with a signal-to-noise ratio $S/N \approx 5$. With a width $\Delta\theta = 1.22''$, the average ring radius, and therefore the distance D , could be determined to better than 1%.

The above example assumed a relatively high X-ray fluence $F_0 = 10^3 \text{ photon cm}^{-2}$; if the fluence is lowered to $F_0 = 10^2 \text{ photon cm}^{-2}$, the ring would have a signal-to-noise ratio of only 0.5 in a single $\Delta t = 2 \times 10^4 \text{ s}$ exposure. However, by taking, say, 50 such exposures in succession and appropriately stacking them to allow for expansion of the ring from one exposure to the next, one could increase the S/N ratio to $0.5\sqrt{50} = 3.5$. RXTE, with a FOV of 1130 deg^2 , detected 8 GRBs in the last 9 months of 1996 (Smith et al. 2002) corresponding to an all-sky event rate of $\sim 320 \text{ yr}^{-1}$. The detected sources had a median 1.5-12 keV fluence of $\sim 10^2 \text{ photon cm}^{-2}$, so we estimate an all-sky event rate of $\sim 10^2 \text{ yr}^{-1}$ of GRBs with $F_0(0.5 - 5 \text{ keV}) > 10^2 \text{ photon cm}^{-2}$. Since the LMC has a projected area of 40 deg^2 , the probability per unit time of a GRB with $F_0(0.5 - 5 \text{ keV}) > 10^2 \text{ photon cm}^{-2}$ behind the LMC is $\sim 0.1 \text{ yr}^{-1}$.

While GRBs could also be used for distance determination for M31 and other spirals, the ring counts $N_r \propto 1/D$ (see eq. (48), and the much smaller angular size (0.8 deg^2 for M31, vs. 40 deg^2 for the LMC) makes it very unlikely to have a suitably bright GRB behind M31. Distance determination using X-ray halos around GRBs will likely be limited to the LMC and SMC.

11. Other Telescopes

XMM-Newton offers a larger aperture than *Chandra*, but its relatively poor angular resolution ($\Delta\theta \approx 6''$) makes it unsuitable for precision distance determination using scattered X-rays. The proposed Constellation X mission is projected to provide an order-of-magnitude increase in collecting area ($A_{\text{eff}} \approx 13000 \text{ cm}^2$ @ 1.5 keV), but current plans call for angular resolution $\Delta\theta \approx 6''$, which would probably preclude accurate distance determination. If the angular resolution were improved to $\sim 1''$, Constellation X would be capable of extragalactic distance determination to local group galaxies using background AGNs with $ES_E \approx 10^{-13} \text{ erg cm}^{-2} \text{ s}^{-1}$.

12. Discussion and Summary

Current distance uncertainties to M31 are of order 10%. Bonanos et al. (2003) are undertaking to use detached eclipsing binaries in M31 to establish the distance with an anticipated accuracy of 5%. We have shown above that a *Chandra* program of extended observations of the field around the background X-ray source 5C 3.76 has the potential to allow the distance to M31 to be determined to an absolute accuracy of $\sim 1\%$, for a 10 Ms observing campaign. In the course of an observing campaign, we estimate a 90% probability that a distance estimate accurate to $\sim \pm 10\%$ would

emerge after 3 Ms (see Table 1); the distance estimate continues to improve as more data accumulates. We caution that our observing time estimates are based on assumed variability properties for 5C 3.76; further observations to characterize its variability should be undertaken. In addition, monitoring of 5C 3.76 would allow a distance-determination campaign to be “triggered” to begin at a time when the source undergoes an outburst (as opposed to our simulations, which started at random times).

A 10 Ms observing campaign would constitute a major commitment of *Chandra* observing time, but would allow determination of the distance to M31 to unprecedented absolute accuracy. There do not appear to be any other methods capable of determining extragalactic distances to such precision in the foreseeable future. A precision determination of the distance to M31 would be of great importance to calibrate the luminosities of stars, and to allow accurate determination of the Hubble constant. The proposed observing campaign would, of course, also provide a census of the X-ray source population in this region of M31 down to lower luminosities than current surveys, as well as information on variability of the point sources.

To summarize our principal conclusions:

1. Realistic X-ray scattering properties for Milky Way interstellar dust have been used to estimate the strength of X-ray scattering halos around distant X-ray point sources seen through foreground galaxies.
2. The X-ray variability properties of AGNs and QSOs are reviewed, and a method for generating simulated light curves is developed (Appendix A).
3. We present a simple method to use X-ray observations of a background AGN and the scattered X-ray halo around it to directly determine the distance to a foreground galaxy. The methodology allows discontinuous observations to be employed. Provided that the fraction of the time lost to the gaps is not large, discontinuous observations will be almost as effective as the idealized continuous observations simulated here.
4. We use simulations to demonstrate the feasibility of direct determination of the distance to M31 using the background BL Lac object 5C 3.76. For the variability properties that we have assumed, a 5 Ms observing campaign with *Chandra* would allow the distance to M31 to be determined to $\sim 4\%$ accuracy, and the absolute distance uncertainty could be reduced to $<1\%$ with a 10 Ms campaign (see Figure 8 and Table 1).
5. We discuss how observations at other wavelengths – H I 21cm and CO 2.6mm aperture synthesis imaging, in particular – can be used to complement the *Chandra* observations.
6. We consider distance determination using the X-ray halo around GRBs. This is a viable method for determining the distance to the LMC or SMC, although GRB statistics suggest that sufficiently bright GRBs occur behind the LMC at a rate of only $\sim 0.1 \text{ yr}^{-1}$.

We thank Bohdan Paczyński for encouraging this study, Adam Dobrzycki, Jochen Greiner, Albert Kong, Frank Primini, Krzysztof Stanek, and Benjamin Williams for helpful correspondence, and Robert Lupton for helpful suggestions and for making available the SM software package. This work was supported in part by NSF grants AST-9988126 and AST-0216105.

A. Synthetic AGN Light Curve

We describe a simple procedure to generate a stochastic light curve with statistical properties resembling X-ray light curves for AGNs.

Let g_j be a sequence of independent random variables with zero mean and unit variance: $\langle g_i \rangle = 0$ and $\langle g_i g_j \rangle = \delta_{ij}$. For times $t_j = t_0 + jh$, let

$$v_j = (1 - e^{-2\lambda})^{1/2} \sum_{i=-\infty}^j g_i e^{-\lambda(j-i)} \quad . \quad (\text{A1})$$

If we set $\lambda = h/\tau$, then

$$\langle v_i \rangle = 0 \quad , \quad (\text{A2})$$

$$\langle v_i v_j \rangle = e^{-|t_i - t_j|/\tau} \quad . \quad (\text{A3})$$

Consider now a (positive-definite) flux given by

$$F(t_j) = a e^{Av_j} \quad (a > 0) \quad . \quad (\text{A4})$$

If the g_j are assumed to be gaussian random variables, then

$$\langle g_j^n \rangle = 0 \quad \text{for } n \text{ odd,} \quad (\text{A5})$$

$$= \frac{n!}{2^{n/2} (n/2)!} \quad \text{for } n \text{ even;} \quad (\text{A6})$$

for this case one can show that

$$\langle F^n \rangle = a^n e^{n^2 A^2/2} \quad \text{for } n = 0, 1, 2, 3, \dots \quad (\text{A7})$$

The r.m.s. fractional variance

$$F_{\text{var}} \equiv \frac{[\langle F^2 \rangle - \langle F \rangle^2]^{1/2}}{\langle F \rangle} = [e^{A^2} - 1]^{1/2} \quad , \quad (\text{A8})$$

so that the coefficient A can be obtained from F_{var} :

$$A = [\ln(1 + F_{\text{var}}^2)]^{1/2} \quad . \quad (\text{A9})$$

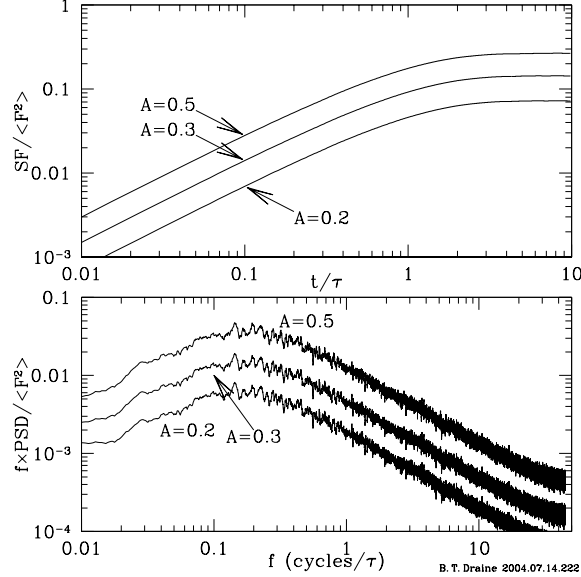


Fig. 9.— Structure function and PSD for synthetic light curves for different values of A .

From (A7) and (A9) we see that the coefficient a in (A4) is

$$a = \langle F \rangle e^{-A^2/2} = \frac{\langle F \rangle}{(1 + F_{\text{var}}^2)^{1/2}} . \quad (\text{A10})$$

The variability can be described by the structure function

$$\text{SF}(\tau) \equiv \langle [F(t) - F(t - \tau)]^2 \rangle \quad (\text{A11})$$

or the power spectral density

$$\text{PSD}(f) \equiv \frac{2(\Delta t)^2}{T_{\text{obs}}} |\tilde{F}(f)|^2 , \quad (\text{A12})$$

where $\tilde{F}(f)$ is the discrete fourier transform of $F(t)$, T_{obs} is the total time span observed, and Δt is the time between measurements.

In Figure 9 we show the structure function and power spectral density obtained from these light curves. The dimensionless quantity $f \times \text{PSD}(f) / \langle F \rangle^2$ peaks at $f_p \approx 1/2\pi\tau$. For $A = 0.3$ the maximum of $f \times \text{PSD}(f) / \langle F \rangle^2$ is ~ 0.015 ; this is in agreement with the maxima of $f \times \text{PSD}(f)$ for the 6 Seyfert galaxies observed by Markowitz et al. The peak frequency $f_p \lesssim 10^{-7}$ Hz for Fairall 9, NGC 5547 and NGC 3516, $\sim 10^{-7}$ Hz for NGC 4151, and $\sim 10^{-6}$ Hz for Ark 564 and NGC 3783.

B. Choice of Annuli

Ideally, annuli would be sufficiently narrow that the variation in time delay across an annulus would be a fraction $\epsilon \ll 1$ of the time τ characterizing fluctuations of the X-ray source. However,

the minimum annulus thickness is set by the angular resolution $\Delta\theta$ of the X-ray imager. Thus we take the outer boundaries to be

$$\psi_j = \psi_1 j^{1/2} \quad \text{for } j \leq j_c \quad (\text{B1})$$

$$= \psi_1 j_c^{1/2} + (j - j_c)\Delta\theta \quad \text{for } j \geq j_c \quad (\text{B2})$$

$$\psi_1 \equiv \left(\frac{2\epsilon c\tau}{D}\right)^{1/2} = 2.88'' \left(\frac{\epsilon}{.01}\right)^{1/2} \left(\frac{\tau}{10^6 \text{ s}}\right)^{1/2} \left(\frac{\text{Mpc}}{D}\right)^{1/2} \quad (\text{B3})$$

$$j_c = \text{nint} \left[\frac{\epsilon c \tau}{2D(\Delta\theta)^2} \right] = \text{nint} \left[2.07 \left(\frac{1''}{\Delta\theta}\right)^2 \left(\frac{\epsilon}{.01}\right) \left(\frac{\tau}{10^6 \text{ s}}\right) \left(\frac{\text{Mpc}}{D}\right) \right] \quad (\text{B4})$$

where $\text{nint}(x)$ is the integer nearest to x .

Note that annuli $j \leq j_c$ are uniformly spaced in time delay δ .

C. Simulation

Our simulated observing campaigns were created as follows. We adopt a value for the time-averaged AGN count rate $\langle F \rangle A_{\text{eff}}$, the AGN correlation time τ , the total exposure time T_{obs} , the scattering optical depth τ (assumed uniform), and the time delay coefficient α , where the extra light travel time for a scattered photon from angle θ is $\alpha\theta^2$.

We assume the observing campaign to capture K images containing the AGN, each for an exposure time T_{obs}/K , where $K = 100$. For simplicity, we assume that there are no time gaps between the images. For an assumed value of the time-averaged point source count rate $\langle F \rangle$ and correlation time τ , we compute a random realization of the AGN light curve $F(t)$ using eq. (A4), using short time steps $h \ll \tau$.

The simulated images are produced as follows: The point source counts N_k are calculated by randomly drawing from a Poisson distribution with expectation value $\int F(t)dt$ integrated over the exposure k .

Because the time delay can vary significantly across a single annulus, we divide each annulus j into a large number of subannuli. Each subannulus has a magnification calculated using equation (9), with the boundaries ψ_j replaced by the boundaries of the subannulus. We assume the background I_{bg} to be uniform across the image. Each subannulus has an expected number of counts during the exposure time Δt_k ; we sum to obtain H_{jk}^0 , the expected number of counts for annulus j during exposure k . We then draw the “observed” counts H_{jk} randomly from a Poisson distribution with expectation value H_{jk}^0 .

The simulated counts N_k and H_{jk} now contain Poisson “noise”. We take N_k and H_{jk} and use the method described in §7 to estimate the background I_{bg} and time delay coefficient α .

D. Statistical Errors

Let m_j^0 be the true magnification of annulus j , let the point source have expected number of counts N_k^0 in time bin k , and let the true background intensity be I_{bg}^0 . Recall that the exposure fraction f_{jk} is the fraction of the time Δt_k for which annulus j was observed.

Suppose we have observed counts H_{jk} in annulus j and time bin k . For the true time delay parameter α_0 , we proceed (as discussed in §7) to construct the halo light curve $G_k(\alpha_0)$. Let

$$A_k(\alpha) \equiv A_{\text{eff}} \sum_j \Omega_j f_{jk}(\alpha) \Delta t_k . \quad (\text{D1})$$

For each time bin k , the observed $G_k(\alpha_0)$ differs from the expected value $[M_k^0 N_k^0 + I_{\text{bg}}^0 A_k(\alpha_0)]$ due to Poisson fluctuations. The expectation values N_k^0 are not known, but the N_k are observed. The true annular magnifications m_j^0 are not known; the estimated annular magnifications $m_j(\alpha_0, I_{\text{bg}}^0)$ and cumulative magnifications $M_k(\alpha_0, I_{\text{bg}}^0)$ are obtained from the observed N_k and the observed $G_k(\alpha_0)$ using eq. (24, 29).

Assuming that we have guessed the correct value of $I_{\text{bg}} = I_{\text{bg}}^0$, we wish to calculate the expectation value $\langle [G_k(\alpha_0) - I_{\text{bg}}^0 A_k(\alpha_0) - M_k(\alpha_0, I_{\text{bg}}^0) N_k]^2 \rangle$ for $1 \leq k \leq K$. Let

$$M_k^0 \equiv \sum_{j=1}^J m_j^0 f_{jk}(\alpha_0) \quad (\text{D2})$$

$$b_{jk}^0 \equiv I_{\text{bg}}^0 A_{\text{eff}} \Omega_j f_{jk}(\alpha_0) \Delta t_k \quad (\text{D3})$$

Then the observed N_k and H_{jk} are

$$N_k = N_k^0 + \nu_k \quad (\text{D4})$$

$$H_{jk} = m_j^0 f_{jk} N_k^0 + b_{jk}^0 + x_{jk} \quad (\text{D5})$$

where ν_k and x_{jk} are independent random variables. The N_k and H_{jk} obey Poisson statistics, thus

$$\langle \nu_k \rangle = \langle x_{jk} \rangle = 0 \quad (\text{D6})$$

$$\langle \nu_k^2 \rangle = \langle \nu_k^3 \rangle = N_k^0 \quad (\text{D7})$$

$$\langle \nu_k^4 \rangle = 3(N_k^0)^2 + N_k^0 \quad (\text{D8})$$

$$\langle x_{jk}^2 \rangle = m_j^0 f_{jk} N_k^0 + b_{jk}^0 \quad (\text{D9})$$

The magnifications $m_j(\alpha_0, I_{\text{bg}}^0)$ are estimated using eq. (24). Expanding in powers of $[\sum_{k=1}^K f_{jk} N_k^0]^{-1}$,

$$m_j = \frac{\sum_{k=1}^K H_{jk} - b_{jk}^0}{\sum_{k=1}^K f_{jk} N_k} \approx m_j^0 + w_j^0 \sum_{k=1}^K x_{jk} - m_j^0 w_j^0 \sum_{k=1}^K f_{jk} \nu_k , \quad (\text{D10})$$

where

$$w_j^0 \equiv \left[\sum_{k=1}^K f_{jk} N_k^0 \right]^{-1} \propto \frac{1}{N} . \quad (\text{D11})$$

We find

$$\begin{aligned} \langle [G_k - I_{\text{bg}}^0 A_k - M_k N_k]^2 \rangle &\approx N_k^0 M_k^0 (1 + M_k^0) + B_k^0 \\ &\quad - 2 [(N_k^0)^2 + (N_k^0)^2 M_k^0 + N_k^0 M_k^0] S_k^0 \\ &\quad + [4(N_k^0)^2 + N_k^0] (S_k^0)^2 \\ &\quad + [(N_k^0)^2 + N_k^0] (T_k^0 + U_k^0) - 2 N_k^0 V_k^0 \quad , \end{aligned} \quad (\text{D12})$$

where

$$B_k^0 \equiv \sum_{j=1}^J b_{jk}^0 \quad (\text{D13})$$

$$S_k^0 \equiv \sum_{j=1}^J m_j^0 w_j^0 f_{jk}^2 \sim \frac{M_k}{N} \quad (\text{D14})$$

$$T_k^0 \equiv \sum_{j=1}^J (w_j^0 f_{jk})^2 \sum_{\ell=1}^K (m_j^0 f_{j\ell} N_\ell^0 + b_{j\ell}^0) \sim \frac{J}{N^2} \left(\frac{M_k N}{J} + \frac{B}{J} \right) \sim \frac{M_k}{N} + \frac{B}{N^2} \quad (\text{D15})$$

$$U_k^0 \equiv \sum_{\ell=1}^K N_\ell^0 \left(\sum_{j=1}^J m_j^0 w_j^0 f_{jk} f_{j\ell} \right)^2 \sim N \left(\frac{M_k}{N} \right)^2 \sim \frac{M_k^2}{N} \quad (\text{D16})$$

$$V_k^0 \equiv \sum_{j=1}^J w_j^0 f_{jk} b_{jk}^0 \sim \frac{B}{K N} \quad (\text{D17})$$

where we have indicated the dependences on M_k , $N \equiv \sum_k N_k^0$, and $B \equiv \sum_k B_k^0$. Eq. (D12) is based on an expansion in powers of $(\sum_k f_{jk} N_k)^{-1} \sim J/N$, and therefore is applicable only if individual annuli are large enough that $\sum_k f_{jk} N_k^0 \gg 1$. Since $M_k^0 \ll 1$, in eq. (D12), the terms in $(S_k^0)^2$ and U_k^0 are normally negligible. The leading order terms are

$$N_k^0 M_k^0 \sim \frac{NM}{K} \quad (\text{D18})$$

$$B_k^0 \sim \frac{B}{K} \quad (\text{D19})$$

$$(N_k^0)^2 S_k^0 \sim \frac{N^2 M}{K^2} \quad (\text{D20})$$

$$(N_k^0)^2 T_k^0 \sim \frac{NM}{K^2} + \frac{B}{K^2} \quad (\text{D21})$$

$$N_k^0 V_k^0 \sim \frac{B}{K^2} \quad (\text{D22})$$

It is also useful to estimate the dispersion of the estimated magnifications m_j around the true values m_j^0 . From eq. (D10):

$$\langle (m_j - m_j^0)^2 \rangle \approx m_j^0 (w_j^0)^2 \sum_k f_{jk} N_k^0 + (w_j^0)^2 \sum_k b_{jk}^0 + (m_j^0 w_j^0)^2 \sum_k f_{jk}^2 N_k^0 \quad . \quad (\text{D23})$$

REFERENCES

Bonanos, A.Z., Stanek, K.Z., Sasselov, D.D., Mochejska, B.J., Macri, L.M., & Kaluzny, J. 2003, AJ, 126, 175

Catura, R.C. 1983, ApJ, 275, 645

Dickey, J.M., & Brinks, E. 1993, ApJ, 405, 153

Dobrzycki, A., Stanek, K.Z., Macri, L.M., & Groot, P.J. 2003, AJ, 126, 734

Draine, B.T. 2003a, ARAA, 41, 241

Draine, B.T. 2003b, ApJ, 598, 1026

Draine, B.T., & Tan, J.C. 2003, ApJ, 594, 347

Ezoe, Y., Iyomoto, N., Makishima, K., & Hasinger, G. 2002, PASP, 54, 981

Fitzpatrick, E.L., Ribas, I., Guinan, E.F., Maloney, F.P., & Claret, A. 2003, ApJ, 587, 685

Freedman, W.L., & Madore, B.F. 1990, ApJ, 365, 186

Gioia, I.M., Henry, J.P., Mullis, C.R., Böhringer, H., Briel, U.G., Voges, W., & Huchra, J.P. 2003, ApJS, 149, 29

Gould, A. 1994 ApJ, 425, 41

Gould, A., & Uza, O. 1998, ApJ, 494, 118

Guinan, E.F., Fitzpatrick, E.L., Dewarf, L.E., Maurone, P.A., Ribas, I., Pritchard, J.D., Bradstreet, D.H., & Giménez, A. 1998, ApJ, 509, L21

Harries, T.J., Hilditch, R.W., & Howarth, I.D. 2003, MNRAS, 339, 157

Hayakawa, S. 1970, Prog. Theor. Phys., 43, 1224

Herrnstein, J.R., Moran, J.M., Greenhill, L.J., Diamond, P.J., Inoue, M., Nakai, N., Miyoshi, M., et al. 1999, Nature, 400, 539

Immler, S., & Wang, Q.D. 2001, ApJ, 554, 202

Laurent-Muehleisen, S.A., Kollgaard, R.I., Feigelson, E.D., Brinkmann, W., & Siebert, J. 1999, ApJ, 525, 127

Lawrence, A., & Papadakis, I. 1993, ApJ, 414, L85

Luks, Th., & Rohlfs, K. 1992, A&A, 263, 41

Markowitz, A., Edelson, R., Vaughan, S., Uttley, P., George, I.M., Griffiths, R.E., Kaspi, S., et al. 2003, *ApJ*, 593, 96

Mauche, C.W., & Gorenstein, P. 1986, *ApJ*, 302, 371

Nilsson, K., Pursimo, T., Heidt, J., Takalo, L.O., Sillanpaeae, A., Brinkmann, W., *A&A*, 400, 95

Overbeck, J.W. 1965, *ApJ*, 141, 864

Paczyński, B. 1997, in *The Extragalactic Distance Scale*, ed. M. Livio, M. Donahue, & N. Panagia (Cambridge: Cambridge Univ. Press), 273

Panagia, N., Golmozzi, R., Macchetto, F., Adorf, H.-M., & Kirschner, R.P. 1991, *ApJ*, 330, L23

Perlman, E.S., Stocke, J.T., Schachter, J.F., Elvis, M., Ellingson, E., Urry, C.M., Potter, M., Impey, C.D., & Kolchinsky, P. 1996, *ApJS*, 104, 251

Predehl, P., Burwitz, V., Paerels, F., Trümper, J. 2000, *A&A*, 357, L25

Predehl, P., & Schmitt, J.H.M.M. 1995, *A&A*, 293, 889

Press, W.H., Rybicki, G.B., & Hewitt, J.N. 1992, *ApJ*, 385, 404

Schmidtobreick, L., Haas, M., & Lemke, D. 2000, *A&A*, 363, 917

Slysh, V.I. 1969, *Nature*, 224, 159

Smith, D.A., Levine, A., Bradt, H., Hurley, K., Feroci, M., Butterworth, P., Golenetskii, G., et al. 2002, *ApJS*, 141, 415

Smith, R.K., Edgar, R.J., & Shafer, R.A. 2002, *ApJ*, 581, 562

Sparks, W.B. 1997, in *The Extragalactic Distance Scale*, ed. M. Livio (Cambridge: Cambridge Univ. Press), p. 281.

Supper, R., Hasinger, G., Lewin, W.H.G., Magnier, E.A., van Paradijs, J., Pietsch, W., Read, A.M., & Trümper, J. 2001, *A&A*, 373, 63

Thim, F., Tamann, G.A., Saha, A., Dolphin, A., Sandage, A., Tolstoy, E., & Labhardt, L. 2003, *ApJ*, 590, 256

Trudolyubov, S., Kotov, O., Priedhorsky, W., Cordova, F., and Mason, K. 2004, *astro-ph/0401227v1*

Trümper, J., & Schönfelder, V. 1973, *A&A*, 25, 445

van den Bergh, S. 2000, *The Galaxies of the Local Group* (Cambridge: Cambridge Univ. Press), 11

Vaughan, S., Willingale, R., O'Brien, P.T., Osborne, J.P., Reeves, J.N., Levan, A.J., Watson, M.G., et al. 2004, ApJ, 603, L5

Wang, Q.D. 2002, MNRAS, 332, 764

West, R.G., Barber, C.R., & Folgheraiter, E.L. 1997, MNRAS, 287, 10

Williams, B.F., Garcia, M.R., Kong, A.H., Primini, F.A., King, A.R., Di Stefano, R., & Murray S.S., 2004, ApJ, 609, 735

Xu, J., Crotts, A.P.S., Kunkel, W.E. 1995, ApJ, 451, 806 (erratum: ApJ 463, 391)

Xu, C., & Helou, G. 1996, ApJ, 456, 152